Vegetation Dynamics Forecasting Using Multispectral Time Series: A Comparative Study of Statistical, Machine Learning, and Deep Learning Models

José Pirangaba Neto[1], **João Fausto Lorenzato**[1], **João Vitor Ataíde**[1]

[1] Rua Benfica, 455 - Escola Politécnica de Pernambuco - Madalena
Caixa Postal 15.064 – 91.501-970 – Recife – PE – Brazil
Programa de Pós-Graduação em Engenharia da Computação
Universidade de Pernambuco (UPE) – Recife, PE – Brazil

{jpsn,jva}@ecomp.poli.br, fausto.lorenzato@upe.br

Abstract. *Due to the high data dimensionality and the availability of chaotic atmospherical data, monitoring and forecasting vegetation dynamics using multispectral pictures presents computational challenges. Using data from Sentinel-2 with more than 3.8 million registrations from January 2018 to December 2025, this paper suggests a method for spatiotemporal analysis of vegetative cover in the Usina União e Indústria, in the state of Pernambuco, Brazil. A preprocessing pipeline based on the HANTS algorithm was created for cloud gap filling and noise reduction, with regularization occurring every 15 days. A comparison study of statistical techniques (ARIMA and SARIMA), machine learning (LightGBM and XGBoost), and deep learning spatiotemporal (Conv3D and ConvLSTM) was then developed and evaluated based on a multistep forecast scenario for 2025. The findings show that machine learning and deep learning are superior, with LightGBM and XGBoost standing out for their superior ability to grasp spatial and temporal patterns. HANTS preprocessing proved crucial for improving temporal consistency and lowering problem complexity. This study's contribution is an integrated evaluation of various predictive techniques in long multispectral time series and a demonstration of the effectiveness of tree-based machine learning models for accurate and computationally efficient vegetation monitoring using remote sensing data.*

1. Introduction

The development of orbital remote sensing technology led to an exploit of the availability and volume of geospatial data [Wen et al. 2025], which changed the monitoring of the earth's surface into a scenario of continuous data capture and high density information. The European Space Agency (ESA) uses satellites such as Sentinel-2[1] to collect multispectral images of the earth's surface with high spatial and temporal resolution [Drusch et al. 2012]. This allows for systematic observation of the dynamics of vegetation, agricultural activities, and environmental changes over time. This scenario has motivated the development of advanced computational methods for analyzing and forecasting time series derived from remote sensing imagery.

Vegetation monitoring is essential for agriculture [Atanasov et al. 2025], environmental management [Aakash et al. 2023], urban planning [Baodong et al. 2009,

[1] https://dataspace.copernicus.eu/data-collections/copernicus-sentinel-missions/sentinel-2

Łochowski et al. 2024], and the assessment of the impacts of climate change [Wang et al. 2024]. Among the products derived from multispectral images, the Normalized Difference Vegetation Index (NDVI) and the Normalized Difference Moisture Index (NDMI) stand out, highly used as indicators of the conditions and healthy of the vegetation due to their ability, respectively, to reduce the effects of lighting variations and surface characteristics, and detect vegetation moisture levels [Sivakumar and Periasamy 2024, Lillesand et al. 2015]. The temporal prediction of these indicators can provide relevant information to support decision making in various sectors, thereby contributing to advanced monitoring and environmental and agricultural change.

However, there are substantial computing difficulties when using time series from remote sensing in forecasting jobs [Aakash et al. 2023][Wen et al. 2025], since the quality of long-term observations is compromised by the intrinsically noisy nature of orbital data, which is influenced by elements including cloud cover, shadows, atmospheric variations, seasonality, and extreme weather occurrences. When these tainted observations are disposed of or masked, fragmented time series with high spatiality, irregular sampling, and temporal gaps are produced. These features make modelling phenological patterns considerably more challenging and violate basic assumptions of many statistical and machine learning algorithms, requiring the employment of strong preprocessing and temporal reconstruction techniques.

Several studies, such [Srivastava and Pant 2020], use statistical models like Autoregressive Integrated Moving Average (ARIMA) to predict NDVI time series, demonstrating their capacity to accurately represent vegetation dynamics. On the other hand, machine learning algorithms, such as the Extreme Gradient Boosting (XGBoost) model presented by [Chang et al. 2024], have been applied to integrate multispectral and multiscale data of agricultural monitoring, achieving high prediction capability. Deep learning models, such as Convolutional Long Short-Term Memory (ConvLSTM) investigated by [Xu et al. 2024], have recently been applied to spatial and temporal relations in remote sensing series, expanding their prediction potential.

In this perspective, this paper proposes a pipeline for analyzing and forecasting multispectral remote sensing time series, employing the Harmonic Analysis of Time Series (HANTS) [Zhou et al. 2015] algorithm for reconstructing and preserving reflectance signals across an eight-year period. Models from the statistics, machine learning, and deep learning categories are compared using regularized data collected at biweekly intervals. As a contribution, this study integrates the evaluation of different modelling paradigms, investigating the impact of harmonic preprocessing and the informational potential of distinct spectral indices in the forecast of vegetation dynamics under atmospheric noisy conditions and a long duration time series.

The remainder of this paper is organized as follows. Section 2 presents the theoretical background, including the spectral indices used, the HANTS reconstruction method, and the forecasting models evaluated. Section 3 describes the study area, data acquisition process, time series reconstruction procedure, experimental setup, and evaluation metrics. Section 4 presents and discusses the experimental results, including the impact of HANTS preprocessing and the comparative performance of statistical, machine learning, and deep learning models. Finally, Section 5 summarizes the main findings and outlines directions for future research.

2. Background

This section introduces the primary ideas employed in this paper, such as the NDVI and NDMI spectral indices, the HANTS algorithm for reconstructing time series, and the types of evaluated forecast models: statistical, machine learning, and deep learning methods.

2.1. Remote sensing and Spectral indices

The data used in this investigation came from the Sentinel-2 constellation, which includes the Sentinel-2A and Sentinel-2B satellites equipped with the MultiSpectral Instrument (MSI) sensor. The mission offers surface reflectance data in visible bands, near-infrared (NIR), and short-wavelength infrared (SWIR). These spectral bands provide complementary information about vegetation characteristics and are widely used for environmental monitoring applications.

Among the spectral indices derived from Sentinel-2 data, NDVI and NDMI were selected for this study. NDVI represents vegetation vigor, whereas NDMI provides information about vegetation moisture conditions.

Equations 1 and 2 use the normalized ratio between spectral bands, which is obtained by dividing the difference between two reflectancies by their sum. This process increases the contrast between the selected bands while reducing the influence of extrinsic factors such as light changes. While NDVI investigates the contrast between the red band (B04) and the NIR (B08) to reflect vegetative vigour, NDMI employs the NIR and SWIR (B11) bands to identify variations associated with vegetation moisture.

$$NDVI = \frac{NIR - Red}{NIR + Red} = \frac{B08 - B04}{B08 + B04} \tag{1}$$

$$NDMI = \frac{NIR - SWIR}{NIR + SWIR} = \frac{B08 - B11}{B08 + B11} \tag{2}$$

2.2. Time Series Reconstruction

Remote sensing time series frequently show missing observations and noise as a result of cloud cover, shadows, and atmospheric phenomena. These interferencies cause temporal gaps and make it difficult to identify vegetation seasonal patterns, compromising the reliability of these data for forecasting.

$$z(t) = a_0 + \sum_{n=1}^{N} \left[a_n \cos(n\omega t) + b_n \sin(n\omega t) \right] \tag{3}$$

Equation 3 shows how HANTS algorithm uses adjustments to enable noise suppression, the reconstruction of missing observations, and the generation of regular temporal series, preserving the current seasoning patterns in the spectral indices. $z(t)$ represents the value of the spectral variable at time t, a_0 is the mean value of the time series, a_n and b_n are the harmonic coefficients, N designates the number of harmonics utilized, and ω is the angular frequency of the modelled cycle.

2.3. Predictive modeling of time series

Statistics models, such as ARIMA and Seasonal Autoregressive Integrated Moving Average (SARIMA), explain temporal dynamics using linear relationships between prior observations, allowing for the representation of trends and seasonality in the series. These

approaches are widely employed in forecasting applications due to their computational interpretability and efficiency.

Machine learning algorithms, such as XGBoost and Light Gradient Boosting Machine (LightGBM), use groups of decision trees to describe nonlinear relationships between variables. Their capacity to capture complicated patterns in large amounts of data has led to their use in time series forecasting and multispectral data analysis.

Deep Learning models such as 3-Dimensional Convolutional layer (Conv3D) and ConvLSTM have been used to detect spatial and temporal correlations in image sequences. While Conv3D extracts spatiotemporal patterns using convolutional three-dimensional methods, ConvLSTM integrates recurrent memory mechanics to describe temporal dependencies across long time periods, making both suitable for remote sensing applications.

3. Methodology

This section outlines the experimental approach utilized in this paper, which includes acquiring data from Sentinel-2, generating and reconstructing temporal time series of NDVI and NDMI, forecasting models, and metrics for result analysis.

3.1. Study Area and Data Acquisition

The research area relates to the adjacent area of Usina União e Indústria, located in the city of Primavera, Pernambuco, Brazil. According to the Köppen classification, the area has a Tropical Savanna climate with a dry summer (AS), with clear seasonal differences between rainy (April to August) and dry (September to March). Sugar cane production dominates the landscape and is the primary agricultural activity in the area. The region was confined to the centre coordinates $-8,34851°$ and $-35,36685°$, the Sentinel-2 Copernicus program provided the data, which included multisprectral images and the Scene Classification Layer (SCL) for the period 2018-2025.

3.2. Preparation and Reconstruction of Time Series

The series were reconstructed from Sentinel-2 images structured in a spatial grade of 113×176 pixels, resulting in a total of 19.888 georeferenced points for the time period studied.

Initially, the NDVI and NDMI indices were calculated for each observation. The layer SCL was then used to detect and filter data that were influenced by clouds, shadows, and other atmospheric phenomena.

The series reconstruction was carried out using HANTS, shown in the algorithm 1, which is based on harmonic decomposition using Fourier Series. In this study, two harmonic components ($N = 2$) were employed to represent the primary sazonality and secondary fluctuations in the vegetation. The correction was made manually for each pixel to preserve the spatial heterogeneity of the study region.

Following reconstruction, the data was resampled to a consistent biweekly period to ensure temporal consistency and allow forecasting algorithms to use them.

Algorithm 1 HANTS-Based Reconstruction of Spectral Time Series

Require: Time series $Z(t)$, quality mask $SCL(t)$, number of harmonics N
Ensure: Reconstructed time series $\hat{Z}(t)$

for each pixel p **do**
  Extract temporal observations $Z_p(t)$
  Build validity mask from $SCL(t)$
  Select observations classified as vegetation or bare soil
  if number of valid observations $<$ minimum required **then**
    Assign unit weights to all observations
  end if
  for each spectral variable **do**
    Initialize harmonic coefficients
    Fit Fourier series using valid observations
    Estimate coefficients $\{a_0, a_n, b_n\}$
    Reconstruct complete series $\hat{Z}(t)$
    Store reconstructed values
  end for
end for
return Reconstructed dataset

3.3. Representative Pixel Selection

Due to the high computational cost of the ARIMA and SARIMA models, which are adjusted individually for each temporal series, these approaches were only tested with two representative pixels.

The first pixel was chosen based on the largest availability of data identified as vegetation by SCL, resulting in a more consistent time serie. The second pixel was chosen based on the highest temporal variation of NDVI and NDMI, indicating a location with high vegetation dynamics.

This technique enables for the evaluation of the statistical models' performance in contrasting situations of vegetation behavior, whereas the other models were trained using the entire dataset of pixels.

3.4. Experimental Setup

The dataset was resampled to a 15-day temporal resolution, generating 24 observations per pixel annually. Historical data from 2018 to 2024 (168 observations per pixel) were used for training, whereas all observations from 2025 (24 observations per pixel) were reserved for testing. The models were evaluated in a multi-step forecasting setting, predicting the complete one-year horizon of 2025.

To ensure transparency and fair comparison, model parameters were systematically defined. Non-seasonal and seasonal lag structures, along with the 24-lag seasonality for ARIMA and SARIMA, were strictly selected based on ADF stationarity testing and ACF/PACF visual inspection detailed in Section 4. For machine and deep learning architectures, feature sets integrated temporal attributes and spectral lag variables. Core hyperparameters, including a learning rate of 0.05, a maximum depth of 6, and 500 es-

timators, were held uniform across all benchmark runs under the multi-step forecasting setup.

3.5. Evaluation Metrics

The performance of the evaluated models was assessed using four complementary metrics: Mean Absolute Error (MAE), which quantifies the average magnitude of prediction errors; Root Mean Squared Error (RMSE), which emphasizes larger errors through quadratic penalization; Symmetric Mean Absolute Percentage Error (SMAPE), which expresses prediction accuracy as a symmetric percentage and is less sensitive to values near zero; and the Pearson Correlation Coefficient (r), which measures the strength of the linear relationship between observed and predicted time series.

4. Results and Discussion

This section presents the findings of NDVI and NDMI time series generated from Sentinel-2 data and reconstructed using the HANTS method. Statistics, machine learning, and deep learning models are compared in light of the 2025 forecast horizon. The performance is evaluated using MAE, RMSE, SMAPE, and Pearson Correlation metrics, as well as comparative analysis between the indices and the various modelling parameters.

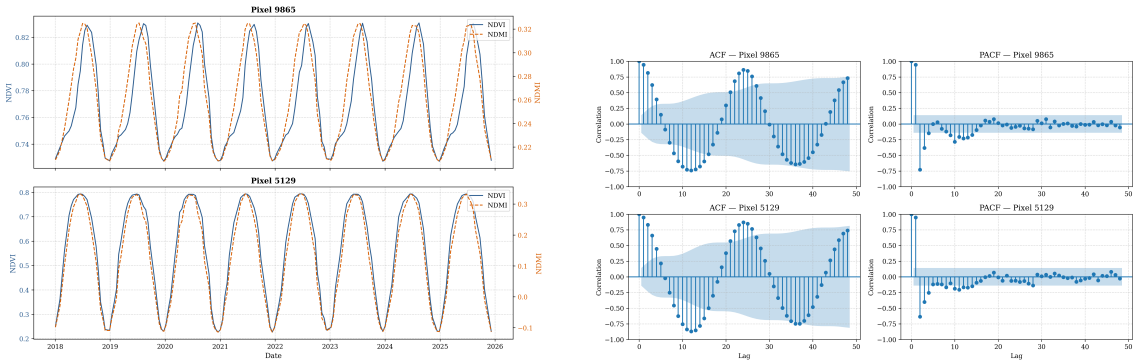
4.1. HANTS' Reconstruction Impact

The use of the HANTS method, resulted in the reconstruction of 2.137.523 observations previously affected by clouds and shadows, amounting to 55% of the original serie. This procedure enabled the recovery of lost data points and the acquisition of a continuous serial analysis.

To evaluate the temporal characteristics of the reconstructed indices, the representative pixels time series are presented in Figure 1a. The reconstructed trajectories shows smooth, highly continuous profiles with clear inter annual stability and zero high-frequency noise from cloud contamination.

To further validate these dynamics, Autocorrelation Function (ACF) and Partial Autocorrelation Function (PACF) analyses were conducted and are shown in Figure 1b. For both pixels, the ACF plots display a smooth sinusoidal pattern with prominent positive correlation spikes recurring every 24 lags, which corresponds directly to a 360-day cycle, confirming that the HANTS algorithm preserved the strong annual seasonality of the local vegetation. Complementarily, the PACF plots show significant positive spikes restricted to the first three lags before truncating within the 95% confidence bounds, demonstrating strong short-term autoregressive dependencies. Together, these structural traits justify the seasonal period selection for SARIMA model and motivate the use of short-term historical lags as input features for tree-based machine learning architectures.

Prior to filtering, cloud contamination, shadow artifacts, and atmospheric interference severely degraded the raw observations, resulting in a valid data coverage of only 44%. Following HANTS reconstruction, missing values were fully gap-filled, achieving 100% valid observation availability across the regularized 15-day temporal grid. Furthermore, to evaluate temporal smoothness, the Mean Temporal Variation—calculated as the average absolute difference between consecutive observations—was assessed as an indicator of artificial noise. Post-processing, this metric dropped drastically from 0.2157 to



(a) Representative pixels time series **(b) ACF and PACF plots**

Figura 1. Post-HANTS reconstructions

0.0247, representing an overall noise reduction of 88.57% and demonstrating a substantial mitigation of abrupt, non-phenological fluctuations.

Figures 2 and 3 demonstrate the influence of HANTS on the NDVI series, showing the elimination of observations relating to clouds and shadows while keeping the vegetation's seasonal pattern.

In addition, figure 4 demonstrates that the reconstruction preserves the spatial organization of the sugar cane culture, correcting only radiometric inconsistencies without changing phenological patterns.

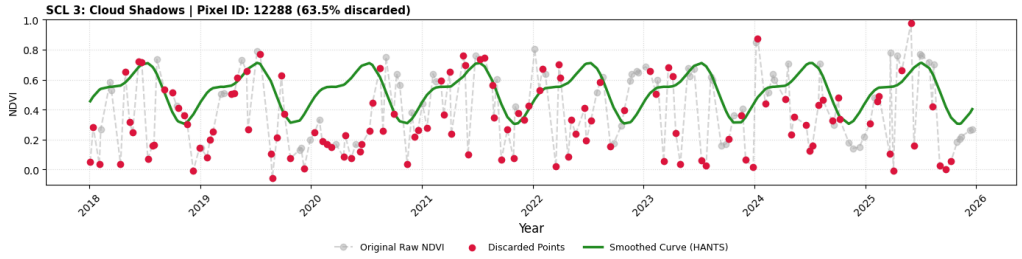


Figura 2. HANTS SCL 3

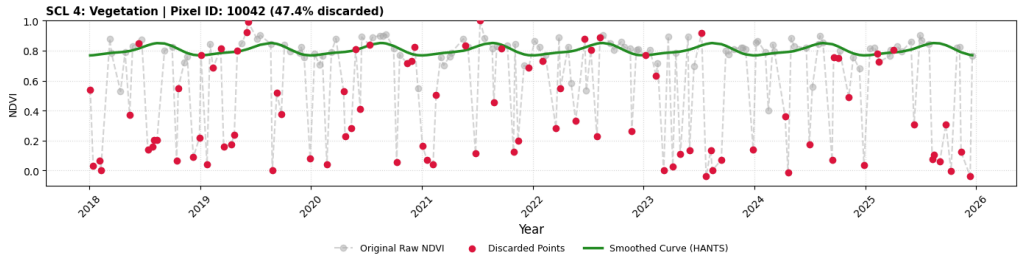


Figura 3. HANTS SCL 4

The findings show that HANTS effectively reconstructs missing observations and reduces atmospheric noise while keeping vegetation seasonality. By minimizing false fluctuations and radiometric inconsistencies, the method enhances the dataset's temporal coherence, resulting in more dependable time series for future statistical, machine learning, and deep learning prediction models.

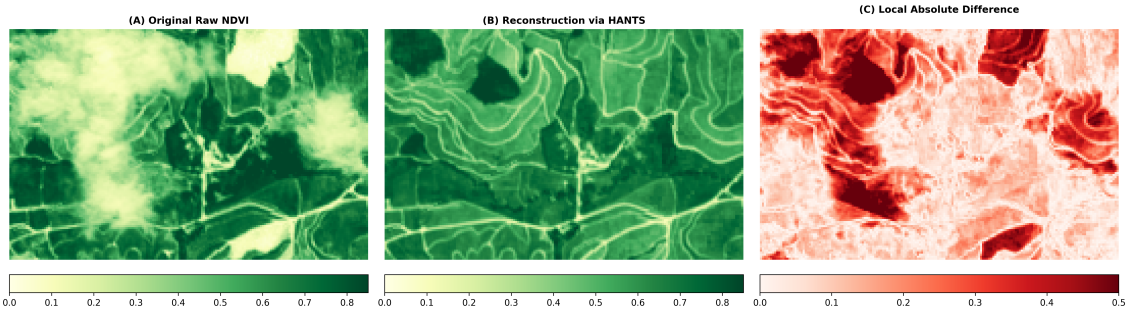
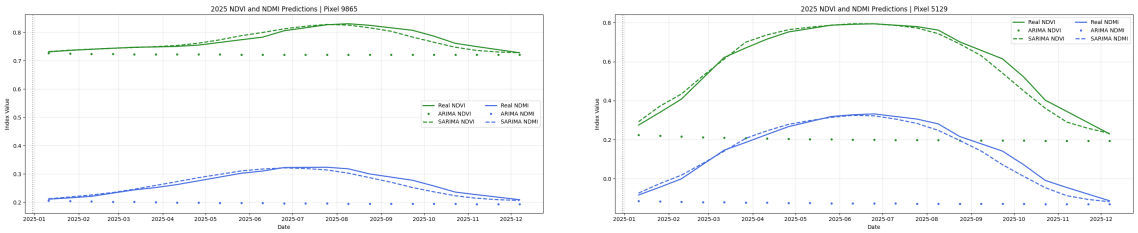


Figura 4. (A) Original NDVI corrupted by atmospheric noise; (B) NDVI reconstructed by the HANTS filter; and (C) Absolute difference of the preprocessing

4.2. Statistic Models Performance

With the parameters $(p, d, q) = (3, 0, 1)$, the ARIMA model was set up to capture short-term linear dependencies using moving average, autoregressive, and differencing components. With the setup $(P, D, Q, s) = (1, 1, 1, 24)$, the SARIMA model explicitly adjusts for the seasonality of the series while taking into account the annual periodicity produced by the biweekly sampling.

As shown in Table 1, seasonality is essential for accurate forecasting. SARIMA consistently outperformed ARIMA and the Simple Moving Average (SMA) baseline, which predicts future values by projecting a constant arithmetic mean of past observations, serving as a non-seasonal benchmark to evaluate whether complex models effectively capture temporal dynamics. On the reliable pixel, SARIMA reduced NDVI MAE to 0.0076, versus 0.0298 for SMA and 0.0505 for ARIMA, while restoring phase alignment. Conversely, static SMA outputs reached 100% NDMI SMAPE on variable pixel, showing non-seasonal baselines fail to track phenology or water stress.



(a) Consistent vegetation pixel **(b) Variable vegetation pixel**

Figura 5. ARIMA and SARIMA predictions for NDVI and NDMI spectral indices

Even though SARIMA also shows improvements in the NDMI scenario, the errors are still higher, suggesting that modelling this variable is more challenging. This implies that whereas NDMI is more susceptible to environmental changes such as soil moisture and precipitation [Gu et al. 2007], which enhances its predictive complexity, while NDVI exhibits a more stable and strongly seasonal behaviour.

Overall, the 2025 predictions across both reliable and variable pixels, shown in figures 5a and 5b, demonstrate a strong annual seasonal component in the region's vegetation dynamics. Consequently, accurate representation is only achieved when seasonality is explicitly modeled.

Tabela 1. SMA, ARIMA, and SARIMA performance on representative pixels

		Reliable Pixel (ID = 9865)				Variable Pixel (ID = 5129)			
Index	**Model**	**MAE**	**RMSE**	**SMAPE (%)**	r	**MAE**	**RMSE**	**SMAPE (%)**	r
NDVI	SMA	0.0298	0.0339	3.84	–	0.1759	0.1929	32.48	–
NDVI	ARIMA	0.0505	0.0612	3.33	-0.5601	0.3850	0.4311	44.80	-0.2291
NDVI	SARIMA	0.0076	0.0103	0.49	0.9548	0.0220	0.0302	2.43	0.9891
NDMI	SMA	0.0352	0.0396	13.33	–	0.1356	0.1510	100	–
NDMI	ARIMA	0.5749	0.5760	59.22	-0.5265	0.7128	0.7384	100	-0.1815
NDMI	SARIMA	0.5100	0.5108	49.55	0.7166	0.4561	0.4592	68.88	0.9766

4.3. Machine Learning Models Performance

The performance of the gradient-based models is very similar, according to the results shown in Table 2. With the same Pearson correlation value ($r = 0.9953$), LightGBM demonstrated nearly comparable performance (2.39%), whereas XGBoost achieved a little advantage in terms of MAPE (2.37%) for NDVI. Similar behaviour is shown with NDMI, with LightGBM slightly outperforming XGBoost in RMSE (0.0119 vs 0.0121).

This performance similarity implies that the variability space of the time series becomes less noisy and more organized following HANTS processing, which promotes the convergence of various boosting techniques towards comparable solutions. As a result, computing efficiency rather than predictive ability becomes the primary factor influencing model differences.

From an operational aspect, LightGBM has an advantage by adopting leaf-wise growth, which saves training time on large-scale datasets like the one employed in this study, comprising of millions of spatiotemporal observations. XGBoost, on the other hand, employs level-wise growth, which raises computing costs while preserving comparable predictive performance.

Tabela 2. LightGBM and XGBoost performance in test dataset

Model	**Index**	**MAE**	**RMSE**	**SMAPE (%)**	r
LightGBM	NDVI	0.0116	0.0152	2.39	0.9953
LightGBM	NDMI	0.0091	0.0119	16.05	0.9944
XGBoost	NDVI	0.0115	0.0153	2.37	0.9953
XGBoost	NDMI	0.0091	0.0121	15.97	0.9942

With lower percentage errors and a strong connection with observed values, spectral index analysis reveals that NDVI behaves more steadily and predictably. While maintaining low absolute errors (MAE and RMSE) and a strong correlation, NDMI exhibits more variability in percentage error (SMAPE).

To summarize, the findings show that both boosting models function almost identically, with LightGBM being marginally more computationally efficient without significantly sacrificing predictive accuracy.

4.4. Deep Learning Models Performance

Significant performance disparities amongst the assessed deep learning architectures are displayed in Table 3. With Pearson correlation values better than 0.988 for both spectral indices (NDVI and NDMI), the ConvLSTM network demonstrated the greatest performance in the deep learning class, demonstrating a high ability to capture the series' spatiotemporal relationships. The Conv3D design, on the other hand, performed noticeably worse, with a significant increase in errors and a loss of correlation that approached zero.

ConvLSTM often obtains RMSEs of 0.0640 (NDVI) and 0.0536 (NDMI), but Conv3D exhibits far greater errors, with RMSEs of 0.1528 and 0.1210, respectively. This behaviour suggests that modelling the temporal dynamics of vegetation requires the inclusion of repeating mechanisms.

The Conv3D architecture's poor performance indicates that it is unable to accurately depict the series' temporal structure, handling the time axis in a largely local and homogeneous manner. This restricts its capacity to simulate long-term seasonal patterns that are typical of the agricultural cycle of sugarcane.

In contrast, ConvLSTM captures both local patterns and long-term interdependence by combining recurrent temporal memory with spatial extraction via convolutions. Its higher stability and improved correlation with the observed series are explained by this mechanism.

Despite this, gradient boosting-based techniques, which demonstrated reduced absolute errors and improved numerical stability, are still shown to be superior to deep learning models. This implies that the tabular structure with temporal attributes and lags is still more effective than dense deep architectures for the dataset under analysis.

Tabela 3. ConvLSTM and Conv3D performance in test dataset

Model	**Index**	**MAE**	**RMSE**	**SMAPE (%)**	r
ConvLSTM	NDVI	0.0531	0.0640	11.19	0.9887
ConvLSTM	NDMI	0.0438	0.0536	44.62	0.9890
Conv3D	NDVI	0.1256	0.1528	28.48	0.3152
Conv3D	NDMI	0.1006	0.1210	71.68	0.3645

5. Conclusion

The results show that the models assessed for predicting the time series of the NDVI and NDMI indices performed significantly differently. When compared to conventional statistical techniques and deep learning architectures assessed in this work, machine learning-based approaches often demonstrated higher predictive capacity.

The significance of seasonality in modelling vegetation time series was brought to light by a comparison of the ARIMA and SARIMA models. SARIMA performed better than ARIMA in every situation examined, showing considerably greater correlations and less errors. With Pearson coefficients better than 0.95, SARIMA showed strong adherence to the seasonal patterns of vegetation, whereas ARIMA was unable to accurately replicate the temporal dynamics of the indices.

The machine learning models produced the greatest results when the entire spatiotemporal dataset was evaluated. With minimal errors and correlation coefficients more than 0.99 for both indices, LightGBM and XGBoost performed nearly identically, exhibiting good predictive accuracy and the capacity to effectively utilize the geographical, temporal, and seasonal information of the data.

With correlations near 0.99, ConvLSTM performed satisfactorily among the deep learning models, while its errors were larger than those of LightGBM and XGBoost. In contrast, Conv3D produced the worst results, showing limitations in capturing the temporal dependencies of the spectral indices for the problem under study, as evidenced by its low correlations and significant errors.

The outcomes additionally emphasize how crucial HANTS preprocessing is for maintaining seasonal vegetation patterns by lowering noise and irregularities in the time series. As a result, the models received more consistent data, which improved correlations and reduced forecast errors.

In conclusion, the findings show that LightGBM and XGBoost outperformed the statistical techniques and deep learning architectures assessed as the best models for predicting NDVI and NDMI indices. They demonstrated potential for operational applications in environmental monitoring, as evidenced by their lower computing cost and higher simplicity of training, as well as their lowest errors and strongest correlations.

Future research should look into hybrid approaches that include statistical techniques, machine learning, and deep learning, as well as meteorological factors and spatiotemporal Transformers. Furthermore, to enable an unbiased comparison, all algorithms should be consistently evaluated on either a single-pixel or full-image basis. To evaluate the methodology's capacity for generalization, it is also advised to apply it to various geographical areas and agricultural crops.

Referências

Aakash, D., K., J., and V., T. (2023). Environmental analysis using remote sensing data. In *2023 International Conference on Recent Advances in Science and Engineering Technology (ICRASET)*, Nagara, India. IEEE.

Atanasov, A., Petrov, P., and Yankova, R. (2025). Exploring the potential of NDVI derivatives for monitoring in precision agriculture. In *2025 International Conference Automatics and Informatics (ICAI)*, Varna, Bulgaria. IEEE.

Baodong, M., Lixin, W., and Shanjun, L. (2009). Analysis to Shenyang urban expansion by using multi-source remote sensing images. In *2009 Joint Urban Remote Sensing Event*, Shanghai, China. IEEE.

Chang, S., Chi, Z., Chen, H. c., Hu, T., Gao, C., Meng, J., and Han, L. (2024). Development of a multiscale XGBoost-based model for enhanced detection of potato late blight using Sentinel-2, UAV, and ground data. *IEEE Transactions on Geoscience and Remote Sensing*, 62.

Drusch, M., Bello, U., Carlier, S., Colin, O., Fernandez, V., Gascon, F., Hoersch, B., Isola, C., Laberinti, P., Martimort, P., Meygret, A., Spoto, F., Sy, O., Marchese, F., and Bargellini, P. (2012). Sentinel-2: ESA's optical high-resolution mission for GMES operational services. *Remote Sensing of Environment*, 120:25–36.

Gu, Y., Brown, J. F., Verdin, J. P., and Wardlow, B. (2007). A five-year analysis of modis ndvi and ndwi for grassland drought assessment over the central great plains of the united states. *Geophysical Research Letters*, 34(6).

Lillesand, T., Kiefer, R. W., and Chipman, J. (2015). *Remote Sensing and Image Interpretation*. John Wiley & Sons, Hoboken, NJ, USA, 7th edition.

Łochowski, P., Cieżkowski, W., and Chormański, J. (2024). Green tracks in urban landscapes: Optimizing vegetation health assessment with UAS NDVI. In *IGARSS 2024 - 2024 IEEE International Geoscience and Remote Sensing Symposium*, Athens, Greece. IEEE.

Sivakumar, S. S. and Periasamy, S. (2024). Damage assessment of cyclone on the mangrove forest using remote sensing techniques. In *2024 IEEE Mediterranean and Middle-East Geoscience and Remote Sensing Symposium (M2GARSS)*, Oran, Algeria. IEEE.

Srivastava, H. and Pant, T. (2020). A time series based study of modis ndvi for vegetation cover. In *2020 IEEE India Geoscience and Remote Sensing Symposium (InGARSS)*. IEEE.

Wang, J., Chen, T., and He, Y. (2024). Application of satellite remote sensing and GIS technology in natural disaster risk assessment. In *2024 IEEE 2nd International Conference on Sensors, Electronics and Computer Engineering (ICSECE)*, Jinzhou, China. IEEE.

Wen, L., Li, P., He, Z., Ma, Z., Luo, D., Jiang, Z., and Liu, W. (2025). An algorithm for satellite remote sensing image compression based on neural network architecture evolution. In *Proceedings of the 2025 IEEE International Geoscience and Remote Sensing Symposium (IGARSS)*, Brisbane, Australia. IEEE.

Xu, L., Cai, R., Yu, H., Du, W., Chen, Z., and Chen, N. (2024). Monthly ndvi prediction using spatial autocorrelation and nonlocal attention networks. 17.

Zhou, J., Jia, L., and Menenti, M. (2015). Reconstruction of global modis ndvi time series: Performance of harmonic analysis of time series (hants). *Remote Sensing of Environment*.